MEDWIN PUBLISHERS
Committed to Create Value for Researchers

Nanomedicine & Nanotechnology Open Access
ISSN: 2574-187X

Facile Co-Precipitation Route for $Zn_{1-X}Cu_xMn_2O_4$ Nanostructure: Synthesis, Characterization, and Magnetic Studies

Shashidharagowda H[1] and Shridhar NM[2]*

[1]Department of Physics, Tontadarya College of Engineering, Gadag, India
[2]Department of Physics, K.L.E. Institute of Technology, Hubballi, India

***Corresponding author:** Shridhar Mathad, Department of Physics, K.L.E. Institute of Technology, Hubballi-Karnataka, India, Email: physicssiddu@gmail.com

Research Article
Volume 5 Issue 3
Received Date: April 17, 2020
Published Date: September 23, 2020
DOI: 10.23880/nnoa-16000197

Abstract

Nano $Zn_{1-x}Cu_xMn_2O_4$ (with x=0.15, 0.25, 0.35, 0.45, and 0.55) ceramics were prepared by co-precipitation method. Formation of tetragonal structure was confirmed by using X-ray diffraction with determination of lattice parameters, crystallite size, dislocation density, and micro strain. The grains sizes and morphology of the samples were unserstood by SEM images. An absorption band of FTIR spectrum employed to supports the formation of structures. VSM studies were done to estimate saturation magnetization (Ms), coercivity (Oe), retentivity (Mr) and magnetic moment (ηB) of the samples. A comparative contemplate carried out with the help of W-H analysis and SSP analysis. A detailed study of influence of copper doping on structural and magnetic properties of synthesized materials is reported.

Keywords: Nanostructures; Manganite; Morphology

Introduction

Nanoparticles have been studied elaborately in recent years due to their size-dependent properties [1-3].The structural, dielectric and electrical properties of nanomaterials are entirely different from their single/poly crystalline and thin film compliments. The high surface to volume ratio of the grains, small size, larger contribution from grains and grain boundary regions; quantum confinement of charges, band structure modification and defects in grains are the few factors which contribute the electrical properties of nanostructure materials [3-6].These difference in nano and bulk materials have immense theoretical and technological importance.

Recently complex manganites (manganese oxides) display a wide range of important electrical and magnetic properties, may be due to the mixed valence states of manganese. Zinc manganite, $ZnMn_2O_4$, is one of the important doped transition-metal oxides due to its potential application. It was found that $ZnMn_2O_4$ is an effective catalyst for reduction of NO to N_2 by several types of hydrocarbons [7,8]. The heat treatment on mixture of Zn and Mn oxides at elevated temperatures led to solid state reaction yielding zinc manganite spinels [9]. $ZnMn_2O_4$ have grabbed a wider attention towards electrochemical, optoelectronic, electronic, mechanical and semiconducting properties which are applicable to the field of sensors, specific memory devices, NTC thermistor, lithium ion batteries as an anode and so on [10-13].

The properties of solid materials are strongly affected by the particle size and morphology. Hence, synthesis of the material in nano range has attracted the researchers deliberately [14-16]. However in $ZnMn_2O_4$, Zn exhibit single oxidation state Zn^{2+}, whereas Mn display Mn^{3+} and Mn^{4+}, which leads to the formation of oxygen vacancy in the material with the temperature variation and which intern

related to relaxation process. Zinc manganite ($ZnMn_2O_4$) has been synthesized by various methods namely solid state reaction [17], hydrothermal method [11,12], sol–gel method and co-precipitation method etc [18].

Usually doping $ZnMn_2O_4$ with small amounts of some other oxides, the electrical, dielectric and magnetic characteristics can be controlled and/or modified [19].In beginning days, $ZnMn_2O_4$ was doped with Bi or Pr [15,19], however, in recent years; it has been doped with elements such as vanadium, manganese, copper, nickel or cobalt etc. The addition of these elements usually produces the formation of secondary phases which are mostly composed by spinel-structure materials [20]. The general formula of such spinels is, AB_2O_4, where A type atoms are located at tetrahedral position (A-site) and B type at octahedral position (B-site).This kind of elemental distribution is known as normal spinel. However, the A and B site ions may swap their positions, partially or totally, producing the so called partial inverse or inverse spinels [21]. As evident from literature that, $ZnMn_2O_4$ crystallizes to normal spinel structure with Zn^{2+} ions at tetrahedral position and Mn^{3+} ions at octahedral position.

However from author's literature knowledge, very little work was carried out with respect to structural, electrical and magnetic studies on copper doped $ZnMn_2O_4$. So the aim of this work was to synthesize copper substituted $ZnMn_2O_4$ ($Zn_{1-x}Cu_xMn_2O_4$ with x=0.15,0.25,0.35,0.45,0.55) by co-precipitation method and to analyze the effect of copper doping on structural characterization using XRD, SEM, FTIR spectra and magnetic studies limited to x = 0.15,0.35,0.55 using VSM spectra for the first time. Also to get more information about micro strain and crystallite size using William-Hall method and size-strain plot method.

Experimental

Preparation of $Zn_{1-x}Cu_xMn_2O_4$

$Zn_{1-x}Cu_xMn_2O_4$ nanoparticles were prepared via co-precipitation method. Zinc chloride, manganese chloride and copper chloride, all of AR grade, were used as source agents for the synthesis. The precursors were purchased from Burgoyne & Burbridges Company, Mumbai, India and were used as received. A desired stoichiometric ratio of precursors were weighed and dissolved in 200ml of distilled water to get the respective solutions which were mixed further. Using magnetic stirrer the mixture was stirred to get liquid solution at ambient temperature. Then liquid NH_3 was added to the solution drop wise to get a pH 7 and stirred for another 1 hour for precipitate formation. The solution was washed repeatedly with distilled water and filtered to get wet brown paste of precipitate. After 24 hours, the dry paste was finely and uniformly powdered using agate mortar and pestle. Using alumina crucible the dry brown powder was sintered at 600°C for 4 h in a muffle furnace to get final black powdered Zinc Copper manganite sample.

Characterization Details

The structural characterization of the synthesized samples was carried out using a Bruker AXS D8 Advance XRD instrument (Detector Si(Li) PSD) using Copper Kα radiation (λ=1.5405Å) at room temperature in the range 0° to 90°at the scanning rate 0.020 per sec to investigate the phase and crystallite size. The Morphology of the samples was studied using SEM (JEOL Model JSM). The FTIR spectral analysis was carried out using spectra obtained on Thermo Nicolet, Avatar370 and the magnetic study was carried out using VSM spectra obtained on Lakeshore 7410 series. The whole process of synthesis and characterization of samples is as shown in (Figure 1).

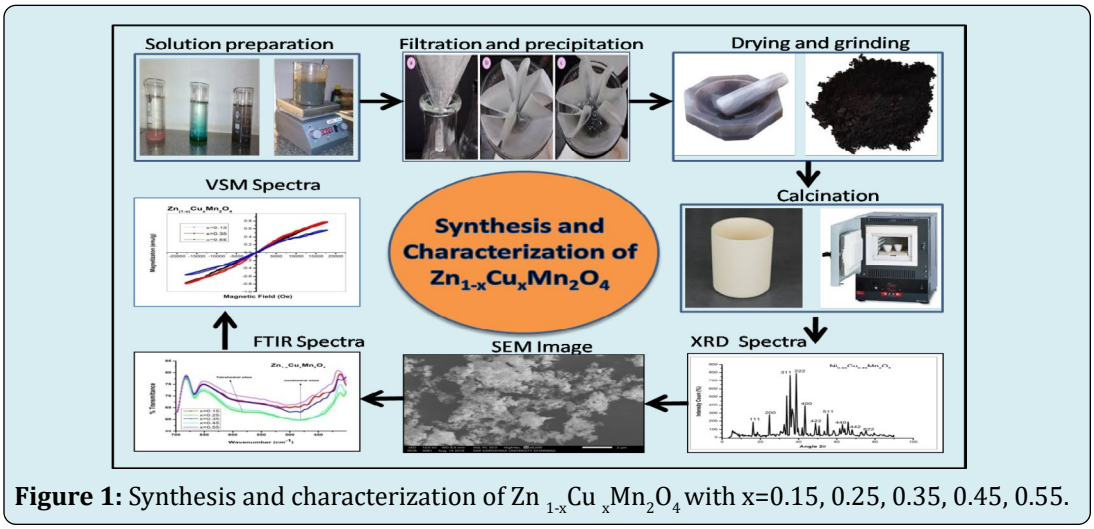

Figure 1: Synthesis and characterization of $Zn_{1-x}Cu_xMn_2O_4$ with x=0.15, 0.25, 0.35, 0.45, 0.55.

Results and Discussion

XRD Structural Analysis

The XRD patterns of $Zn_{1-x}Cu_xMn_2O_4$ with x=0.15, 0.25, 0.35, 0.45, 0.55 are shown in (Figure 2) for all samples, the same pattern was observed with well developed (*h k l*) reflections with preferential orientation at (1 2 1) and (0 2 0) plane direction. The spectra were well indexed with the help of JCPDS file 96-901-2843, which confirms the tetragonal spinel structure with space group of I41/amd [16]. The $Zn_{1-x}Cu_xMn_2O_4$ shows tetragonal symmetry at room temperature due to John-Tellar effect on Mn^{3+} ions as evident [22,23]. The samples showed high purity as there is no evidence of impurities from starting materials was seen in the patterns. The spinel lattice of the samples $Zn_{1-x}Cu_xMn_2O_4$ consists of O^{2-} anions, form a close-packed tetragonal lattice in which the Zn^{2+} and Cu^{2+} cations are located in tetrahedral sites (A sites) and Mn^{3+} are located in octahedral sites (B sites), respectively, while non J-T cations Mn^{2+} and Mn^{4+} take mixed positions. Due to their electronic configuration ($3d^{10}$), the Zn^{2+} ions are highly stabilized at tetrahedral sites of the structure. They form ionocovalent bounding with the oxygen anions [24].

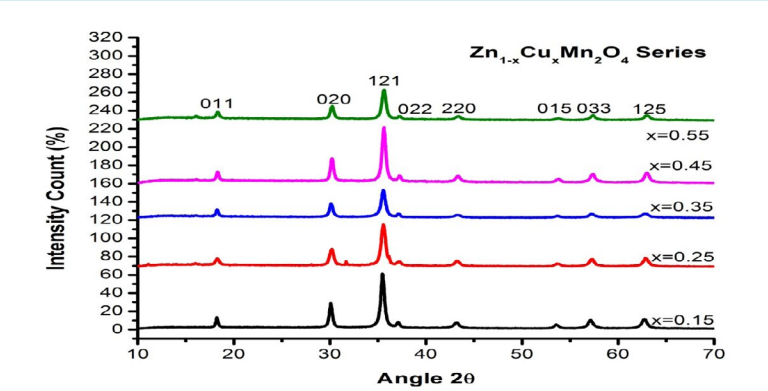

Figure 2: XRD patterns of $Zn_{1-x}Cu_xMn_2O_4$ with x=0.15, 0.25, 0.35, 0.45, 0.55.

The lattice parameters a and c for tetragonal crystal structure were calculated with the help of

$$d = \frac{1}{\sqrt{\frac{h^2}{a^2} + \frac{k^2}{b^2} + \frac{l^2}{c^2}}}$$

where a = b ≠ c (1)

Crystallite size *D* was detrmined using equation of Debye–Scherer

$$D = 0.9\lambda/\beta\cos\theta \quad (2)$$

where λ is the wavelength of radiation used, (λ = 1.5406 Å), β is the full width half maximum (FWHM) of diffraction peak, and θ is the Bragg's angle. The defect present within crystal structure (so called irregularity), which greatly affect the material properties is called as dislocation. Dislocation density is the number of dislocations per unit volume of crystalline material. The parameters; dislocation density ρ_D and micro strain ε were determined using.

$$\rho_D = \frac{1}{D^2} \quad (3)$$

$$\varepsilon = \beta\cos\frac{\theta}{4} \quad (4)$$

While x-ray density (Δ_x) was got by

$$\Delta_x = \frac{4M}{NV} \quad (5)$$

Where M is the molecular weight of each composition, N is the Avogadro's number and V is unit cell volume.

The calculated values of lattice parameters of synthesized tetragonal samples are as a = 5.921 Å to 5.835Å. and c = 8.969Å to 8.373Å, the unit cell volume V=303.49Å^3 to 289.75Å^3 and average crystallite size D = 21.94 nm to 16.98 nm as presented in Table 1. The values of lattice parametres nonlinearly varies with copper due to John-Teller distortions of Mn^{3+} ions at octahedral sites.With the increase of copper, the unit cell volume V and crystallite size D values decreases slightly due to difference in cationic radii of Cu^{2+} (0.073nm), Zn^{2+} (0.074nm) and Mn^{3+} (0.083nm) in octahedral sites [22,23]. Discussions reported in Kshirasagar *et al* suggests

that synthesized samples $Zn_{1-x}Cu_xMn_2O_4$ shows tetragonal structure from x=0.15 to x=0.55 due to J-T effect which could be removed once x tends to 1. Also it is assumed that the values of x-ray density, dislocation density and micro-strain are certainly affected by J-T effect as evident from their values as reported in (Table 1).

x	a Å	c Å	Unit cell Volume Å^3	Crystallite size D nm	Micro strain ε x 10-3	Dislocation density ρ_D x 10^{15} /m^2	X ray density D_x g/cm^3
0.15	5.859	8.840	303.49	21.94	1.799	2.077	5.23
0.25	5.753	8.969	296.90	20.94	1.762	2.280	5.34
0.35	5.921	8.373	293.61	20.48	2.184	2.383	5.39
0.45	5.910	8.378	292.67	18.98	1.929	2.775	5.33
0.55	5.835	8.509	289.75	16.98	2.158	3.468	5.22

Table 1: Calculated values of Lattice parameter (a and c), Unit cell volume (V), Crystallite size (D), Micro strain (ε), Dislocation density ρ_D and X-ray Density (D_x).

Williamson - Hall Plot and Size-Strain Plot Method

Lattice strain η and average crystalline size D were determined using the equation of Williamson–Hall [25]:

$$\frac{\beta\cos\theta}{\lambda} = \frac{1}{D} + \frac{n\sin\theta}{\lambda} \quad (6)$$

The above expression could be expressed as $y = mx + c$ where $m = \eta$ and $c = 1/D$, so the linear plot of $\beta\cos\theta$ *V/s*. $\sin\theta$ produces the lattice strain η as slope and $1/D$ as intercept as reflected in (Figure 3). The Table.2 is filled with the calculated and graphical values of mean crystallite size D and lattice strain η, *which are nearly in* agreement with each other.

There is a prominent method to find the isotropic nature and micro-strain, called as "size-strain plot" (SSP), which uses average values of size-strain parameters. The benefit of this method is that, less credence will be given to the information collected from higher angle reflections having lower precision, as shown in (Figure 4). We consider that the "crystallite size" is expressed with Lorentzian function and the "strain profile" with Gaussian function [26-28]. Consequently, we have:

$$\left(d_{hkl}\beta_{hkl}\cos\theta\right)^2 = \frac{K\lambda}{D}d_{hkl}^2\beta_{hkl}\cos\theta + \left(\frac{E}{2}\right)^2 \quad (7)$$

where K is a constant which renders on particles shape (for spherical particles $K = 3/4$). The (Table 2) represents the comparison between different values got from W-H plot and SSP plot.

x	Crystallite size (D) nm			Micro strain (ε) x 10^{-3}		
	From W-H plot	From formula	From S S Plot	From W H graph	From formula	From S S Plot
0.15	48.60	21.94	28.11	9.89	1.80	18.67
0.25	15.71	20.94	11.98	6.61	1.76	15.18
0.35	52.22	20.48	24.02	15.03	2.18	25.13
0.45	40.54	18.98	15.94	9.93	1.93	3.25
0.55	25.84	16.98	13.56	6.77	2.16	3.86

Table 2: Comparison of crystallite size D and micro strain ε values calculated from W-H plot and Size-Strain plot.

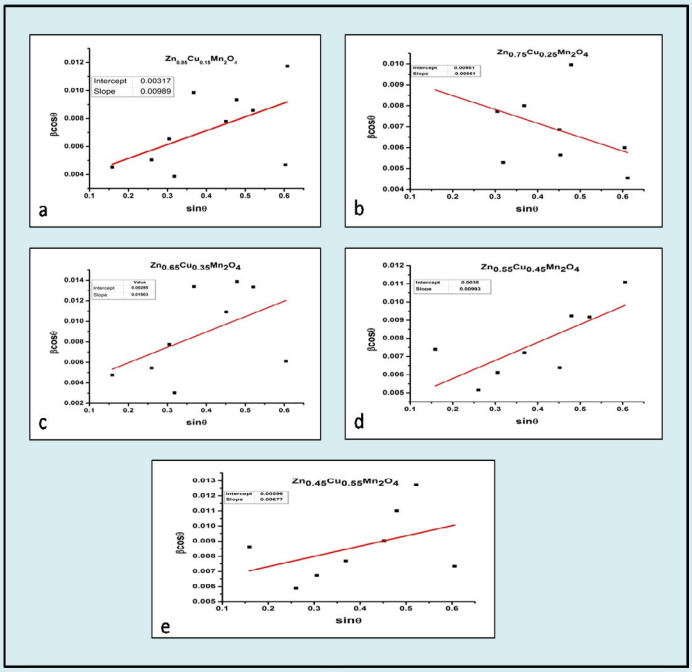

Figure 3: Williamson-Hall Plot βcosθ V/s sinθ for $Zn_{(1-x)}Cu_xMn_2O_4$ samples with x=0.15,0.25,0.35,0.45,0.55.

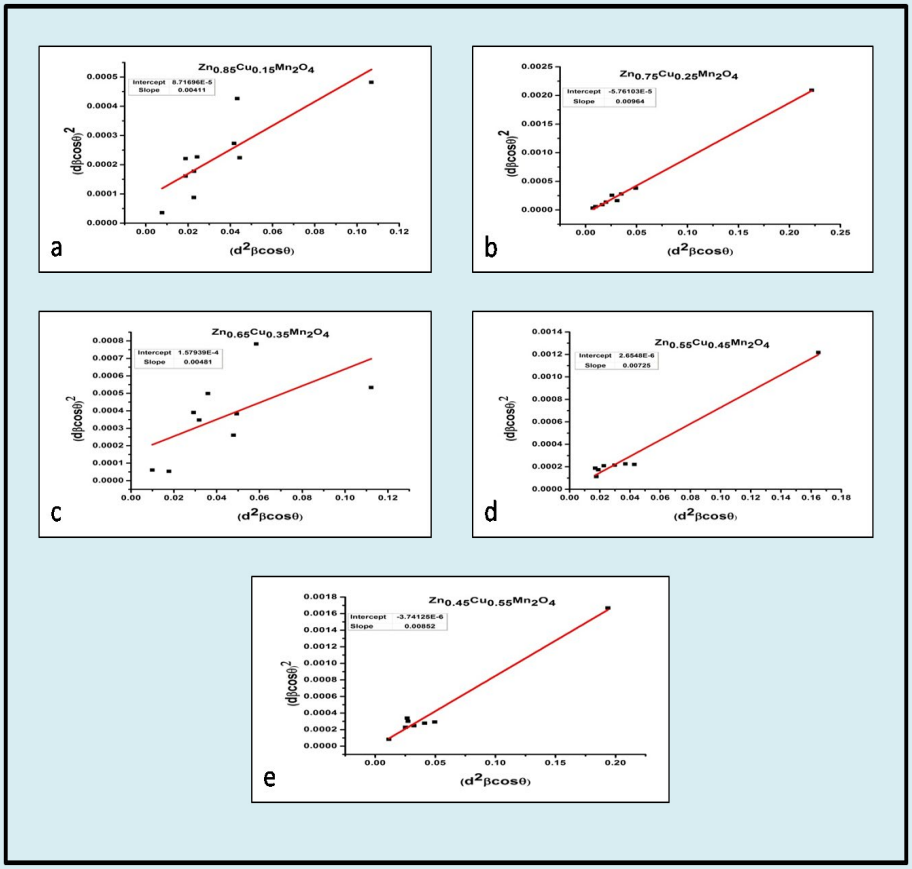

Figure 4: Size-Strain Plot $(d\beta\cos\theta)^2$ V/s $(d^2\beta\sin\theta)$ for $Zn_{(1-x)}Cu_xMn_2O_4$ with x=0.15,0.25,0.35,0.45,0.55.

FTIR Analysis

The confirmation of crystal structure and infrared spectral analysis was carried with the help of FTIR spectra of the synthesized samples. The spectra were taken in the range 700-400 cm^{-1} as shown in (Figure 5). The position of transmission bands with frequency are tabulated in (Table 3). There exist two main absorption bands ν_1 and ν_2 corresponding to the stretching vibration of tetrahedral (A-site) and octahedral (B-sites) positions around 600 cm^{-1} and 480 cm^{-1} [29]. The band frequencies (ν_2) around 480 cm^{-1} are associated with an internal bending mode of MnO_6 octahedral and the band frequencies (ν_1) around 600cm^{-1} are attributed to phase stretching mode of Mn-O, varies nonlinearly due to John- Teller distortions [30,31]. Also the curve becomes more pronounced for larger x values indicating the effect of copper at both the sites. The increase in Mn-O vibration frequency from 582 cm^{-1} to 599 cm^{-1} indicates strong coupling constant which tends to shorter bond length and decrease in lattice constant. The values of ν_1 are higher than ν_2, indicates that the normal vibration mode of the tetrahedral complexes is higher than that of the corresponding octahedral sites. This may be due to a shorter bond length in the tetrahedral site compared to octahedral one. Due to nano grain sizes, there is a shift in IR frequencies as compared to FTIR bands of bulk materials also there is a degradation of crystal symmetry. Nano size grains are showing some disorder, as their atomic arrangements on the boundaries differ greatly from that of bulk crystals both in co-ordination number and bond lengths [32].

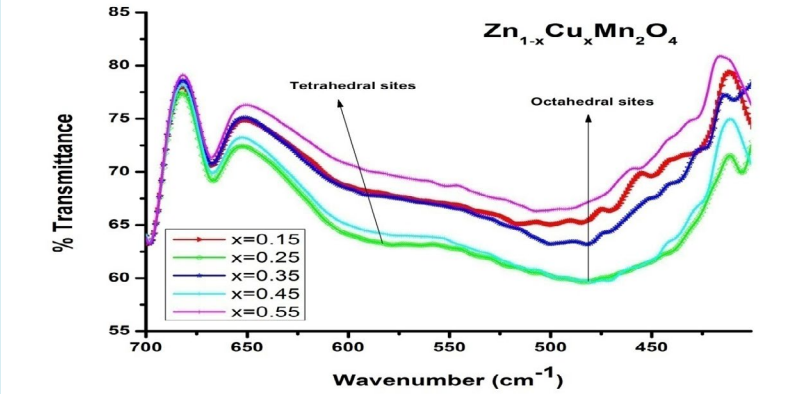

Figure 5: FTIR spectra of $Zn_{1-x}Cu_xMn_2O_4$ with x=0.15, 0.25, 0.35, 0.45, 0.55.

Concentration x	ν_1 cm^{-1}	ν_2 cm^{-1}
0.15	590.72	483.77
0.25	583.02	485.56
0.35	590.12	481.97
0.45	585.34	485.56
0.55	594.90	490.34

Table 3: Positions of IR Transmittance bands of $Zn_{1-x}Cu_xMn_2O_4$ Series.

Surface Morphology

The surface analysis was carried out using SEM (Scanning Electron Microscope). The surface micrographs of synthesized samples are shown in (Figure 6). The images showed highly porous, less densed, agglomerated and algea structured grains.The grains sizes of the samples ranging from 3.934 µm to 13.73 µm measured using ImageJ software. The images revels that the samples are less dense and the particle size distribution was significantly broad, due to an irregular growth of the particles. The morphological characterization showed that the homogeneity and grains size continuously increases with copper addition due to ionic radii of Cu^{2+} (0.073nm), Zn^{2+} (0.074nm) and Mn^{3+} (0.083nm).

The porosity of samples goes on decreases as x increases and at x=0.55 the concentration of both Cu^{2+} and Zn^{2+} become nearly equal to each other, by which the material looks to be more denser.

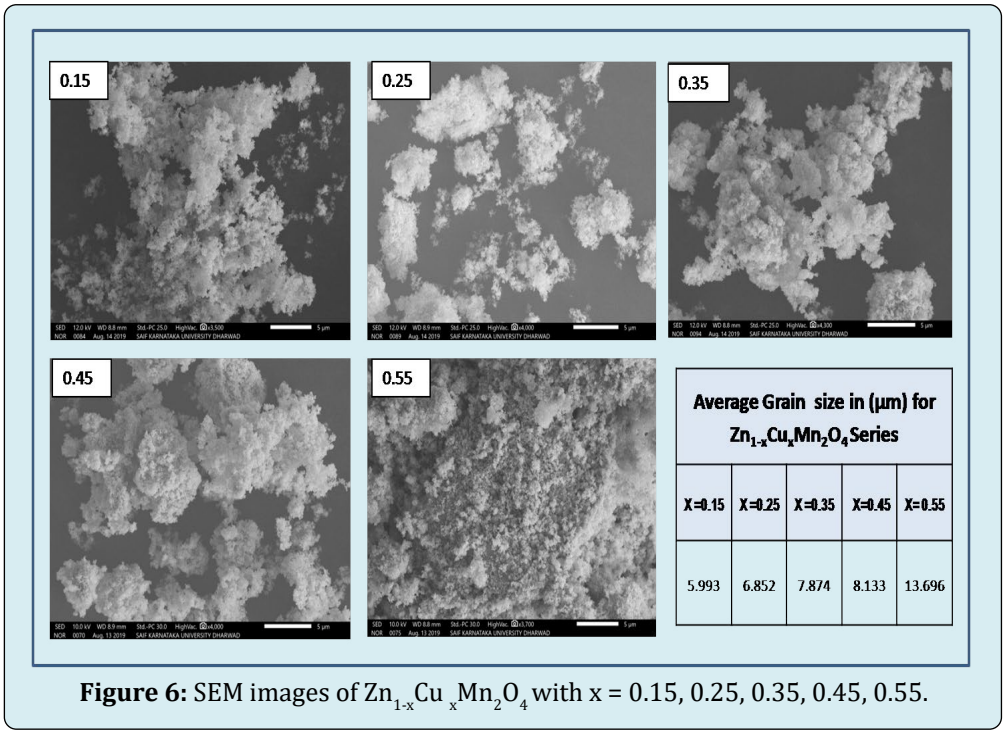

Figure 6: SEM images of $Zn_{1-x}Cu_xMn_2O_4$ with x = 0.15, 0.25, 0.35, 0.45, 0.55.

Magnetic Study

Vibrating sample magnetometer was used to investigate the magnetic properties of synthesized $Zn_{1-x}Cu_xMn_2O_4$ with x = 0.15, 0.35, 0.55 at room temperature. (Figure 7) shows VSM plots. The values of saturation magnetization (Ms), coercivity (Oe), retentivity (Mr) and magnetic moment (η_B) of the samples are listed in Table 3. The magnetic moment/ formula unit in Bohr magneton (μ_B) was determined by following equation [33].

$$\text{Magnetic moment } \eta_B = \frac{M * Ms}{5585} \quad (8)$$

Where M is the molecular weight of a each composition and Ms is the saturation magnetization (emu/gm).

All the samples showed almost narrow hysteresis loops, indicating slight ferromagnetic and antiferromagnetic nature. The concurrent presence of Mn^{4+}, Mn^{3+} and Mn^{2+} ions are liable for ferromagnetic properties shown by the samples under investigation, which give rise to ferromagnetism in terms of double-exchange mechanism. Zn and Cu ions acting as retardant of the magnetic interaction between the manganese ions [16]. According to Anuradha et al [33] the maximum magnetization was observed for the sample with lowest particle size, confirms the increase in ferromagnetism and decrease in particle size with Cu content as apparent from (Figure 7 and Table 4). Also the discussions from Fierro et al [22] suggests that $Zn_{1-x}Cu_xMn_2O_4$ compounds shows antiferromagnetic nature due to partial replacement of Cu^{2+} with Zn^{2+} ions in the A site of the spinel structure. This clearly confirms the introduction of Cu^{2+} ions into Zinc manganites greatly affects the magnetic properties. The magnetic study of all the samples indicates that, the variation in saturation magnetization, retentivity, coercivity and magnetic moment is due to the substitution of copper to $ZnMn_2O_4$ and the sites preference energy also play important role in magnetization [34].

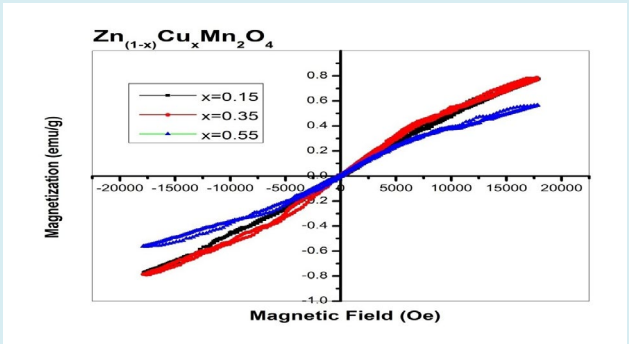

Figure 7: Magnetization (Ms) V/s Magnetic field (Oe) for $Zn_{1-x}Cu_xMn_2O_4$ with x = 0.15, 0.35, 0.55.

Concentration x	0.15	0.35	0.55
Crystallite size (D) nm	21.94	20.48	16.98
Coercivity (Oe)	23.22	15.91	7.102
Magnetization (Ms) emu/g	0.774	0.789	0.561
Retentivity (Mr) emu/g x10^{-3}	5.58	3.97	0.356
Magnetic moment η_B	0.033	0.034	0.024

Table 4: Calculated values of Crystallite size (D), Coercivity (Oe), Saturation Magnetization (Ms), Retentivity (Mr) and magnetic moment ($\eta_{B)}$ for $Zn_{1-x}Cu_xMn_2O_4$ with x = 0.15, 0.35, 0.55.

Conclusion

The co-precipitation method was used to successfully synthesize $Zn_{1-x}Cu_xMn_2O_4$ samples. The XRD patterns confirmed the formation of tetragonal phased $Zn_{1-x}Cu_xMn_2O_4$ with the space group I41/amd. With increase in copper content the unit cell volume V and crystallite size D values decreases significantly due to difference in cationic radii in octahedral sites in the structure.It was evident from the results that lattice parametres, x-ray density, micro strain and dislocation density varies nonlinearly with copper content due to John-Teller distortions of Mn^{3+} ions at octahedral sites. The XRD patterns showed (121) and (020) planes have strong preferential orientation for all the samples. Crystalline structure was correlated by Williamson-Hall plot and Size-Strain Plot methods. SEM image showed agglomerated, porous and less densed algea structured grains, with sizes ranging from 3.934μm to 13.73μm.The effect of copper clearly seen in the images.Through the FTIR spectra the spinel tetragonal formation was confirmed. VSM spectral inspection showed the effect of copper substitution on magnetic properties of the samples in terms of partial ferromagnetic and antiferromagnetic nature.

References

1. Mousavand T, Ohara S, Umetsu M, Zhang J, Takami S, et al. (2007) Hydrothermal synthesis and in situ surface modification of boehmite nanoparticles in supercritical water. Fluids 40(3): 397-404.

2. Shchukin D G, Sukhorukov G B (2004) Nanoparticle Synthesis in Engineered Organic Nanoscale Reactors. Adv Mater 16(8): 671-682.

3. Oh J, Lee J, Kim S J, Han S B, Park K (2010) TiO_2 Branched Nanostructure Electrodes Synthesized by Seeding Method for Dye-Sensitized Solar Cells†. Chem Mater 22(3): 1114-1118.

4. Nomura T, Mori T, Arima H, Konishi Y (2009) Shape and size control of barium chromate nanoparticles using reverse micelle. Adv Powder Technol 20(1): 101-105.

5. Li Y, Guo Y, Tan R, Cui P, Li Y, et al. (2009) Synthesis of SnO_2 nano-sheets by a template-free hydrothermal method. Mater. Lett 63(24-25): 2085-2088.

6. Kurien S, Mathew J, Sebastian S, Potty S N, George K C (2006) Dielectric behavior and ac electrical conductivity of nanocrystalline nickel aluminate. Mater. Chem. Phys 98 (2-3): 470-476.

7. Ferraris G, Fierro G, Jacono ML, Inversi M (2002) A study of the catalytic activity of cobalt–zinc manganites for the reduction of NO by hydrocarbons. Appl Catal B Environ 36(4): 251-260.

8. Ferraris G, Jacono M L, Dragone R, Ferraris G, Andreozzi B, et al. (2005) Fe–Zn manganite spinels and their carbonate precursors: preparation, characterization and catalytic activity. Appl Catal B Environ 57(3): 153-165.

9. Selim MM, Deraz NM, El-Asmy AA, El-Shafey O (2010) Synthesis, characterization and physicochemical properties of nanosized Zn/Mn oxides system. J. Alloys Compds 506(2): 541.

10. Gherbi R, Bessekhouad Y, Trari M (2016) Structure, optical and transport properties of Mg-doped ZnMn2O4. J. Alloys Compd 655: 188-197.

11. Zhang P, Li X, Zhao Q, Liu S (2011) Synthesis and optical property of one-dimensional spinel ZnMn2O4 nanorods. Nanoscale Res. Lett 6(1): 323.

12. Lakshmi S V, Pauline S (2014) Structural, Morpological and Optical Properties of Hetarolite- Znmn2o4 Nano Particle by Hydrothermal Method. Int J Sci Res 3: 8-9.

13. Deng Y, Tang S, Zhang Q, Shi Z, Zhang L, et al. (2011) Controllable synthesis of spinel nano-ZnMn2O4via a single source precursor route and its high capacity retention as anode material for lithium ion batteries. J Mater Chem 21(32): 11987-11995.

14. Jadhav RN, Puri V (2013) Effect of Film Thickness and pH of Zinc Manganite on Microwave Absorption and Complex Permittivity. Journal Synthesis and Reactivity

in Inorganic, Metal-Organic, and Nano-Metal Chemistry 44: 1426-1428.

15. Francisco Méndez-Martínez, Federico González, Enrique Lima, Pedro Bosch, Heriberto Pfeiffer (2010) $Znx_{-1}CuxMn_2O_4$ Spinels; Synthesis, Structural Characterization and Electrical Evaluation. J Mex Chem Soc 54(1): 2-6.

16. Bessekhouad Y, Trari M (2002) Photocatalytic hydrogen production from suspension of spinel powders AMn_2O_4 (A=Cu and Zn). Int J Hydrogen Energy 27: 357-362.

17. Rosenberg M, Nicolau P, Manaila R, Pausescu P (1963) Preparation, electrical conductivity and tetragonal distortion of some manganite-systems. J Phys Chem Solids 24(12): 1419-1434.

18. Clarke D R (2014) Varistor Ceramics. J Am Ceram Soc 82: 485-502.

19. Kuo CT, Chen CS, Lin IN (1998) Microstructure and Nonlinear Properties of Microwave-Sintered ZnO-V_2O_5 Varistors: II, Effect of Mn_3O_4 Doping. J Am ceram Soc 81(11): 2949-2948.

20. West AR (1990) Solid State Chemistry and its Application, J. Wiley &Sons, New York.

21. Kshirsagar ST, Biswas AB (1967) Crystallographic studies of some mixed manganite spinels. J Phys Chetn Solids Pergamon Press 28(8): 1493-1499.

22. Fierro G, Morpurgo S, Lo Jacono M, Inversi M, Pettiti I (1981) Preparation, characterisation and catalytic activity of Cusingle bondZn-based manganites obtained from carbonate precursors. Applied Catalysis A: General 166(2): 407-417.

23. Guillemet Fritscha S, Chanela C, Sarrias J, Bayonnea S, Rousset A, et al. (2000) Structure, thermal stability and electrical properties of zinc manganites. Solid State Ionics 128(1-4): 233-242.

24. Zak AK, Abrishami ME, Majid WH Abd, Yousefi R, Hosseini SM (2011) Effects of annealing temperature on some structural and optical properties of ZnO nanoparticles prepared by a modified sol-gel combustion method. Ceram Inter 37(1): 393-398.

25. Kulkarni AB, Mathad SN (2018) Synthesis and Structural Analysis of Co–Zn–Cd Ferrite by Williamson–Hall and Size–Strain Plot Methods. International Journal of Self-Propagating High-Temperature Synthesis 27(1): 37-43.

26. Prabhu YT, Rao KV, Kumar VSS, Kumari BS (2014) X-Ray Analysis by Williamson-Hall and Size-Strain Plot Methods of ZnO Nanoparticles with Fuel Variation. World Journal of Nano Science and Engineering 4: 21-28.

27. Shashidhar G, Mathad SN (2018) Synthesis and Structural Analysis of $Ni_{0.45}Cu_{0.55}Mn_2O_4$ by Williamson–Hall and Size–Strain Plot Methods. Ovidius University Annals of Chemistry 29(2).

28. Henderson CMB, Charnock JM, Plant DA (2007) Cation occupancies in Mg, Co, Ni, Zn, Al ferrite spinels: a multi-element EXAFS study. J. Phys. Condens. Matter 19(7): 076214.

29. Kumar N, Kishan H, Rao A, Awana VPS (2010) Structural, electrical, magnetic, and thermal studies of Cr-doped $La_{0.7}Ca_{0.3}Mn_{1-x}Cr_xO_3$ ($0\leq x\leq 1$) manganites. Journal of Applied Physics 107: 083905.

30. Kolat V, Gencer H, Gunes M, Atalay S (2007) Effect of B-doping on the structural, magnetotransport and magnetocaloric properties of $La_{0.67}Ca_{0.33}MnO_3$ compounds. Materials Science and Engineering: B 140(3): 212-217.

31. Hosseini SA, Niaei A, Salari D, Nabavi SR (2012) Nanocrystalline AMn_2O_4 (A=Co, Ni, Cu) spinels for remediation of volatile organic compounds-synthesis, characterization and catalytic performance. Ceramics International 38(2): 1655-1661.

32. Kambale RC, Shaikh PA, Kamble SS, Kolekar YD (2009) Effect of cobalt substitution on structural, magnetic and electric properties of nickel ferrite. J. Alloys Comp 478(1-2): 599-603.

33. Anuradha KN, Koushalya PR, Bhat SV (2015) Size Dependent Magnetic Properties of Nd0.7Ca0.3MnO3 Nanomanganite. IOP Conf. Series: Materials Science and Engineering 73: 012007.

34. Hankare PP, Pandav RS, Patil RP, Vader VT, Garadkar KM (2012) Synthesis, structural and magnetic properties of copper substituted nickel manganite. Journal of Alloys and Compounds 544: 197-202.